STUDIES OF TRANSFORMATIONS OF INORGANIC CONSTITUENTS IN A TEXAS LIGNITE DURING COMBUSTION

C.J. Zygarlicke, E.N. Steadman, S.A. Benson, and W.H. Puffe
University of North Dakota Energy and Mineral Research Center
Box 8213 University Station
Grand Forks, ND 58202.

INTRODUCTION

The effects of coal composition and combustion conditions on the mechanisms of ash formation are being investigated at the Energy and Mineral Research Center (EMRC). The objective of the study is to develop a unified understanding of formation of ash components during pulverized coal combustion. This understanding will aid in predicting the formation of ash deposits, erosion of boiler parts and formation of fine particulate that is difficult to collect.

The approach used to obtain a better understanding of inorganic transformations that take place during combustion of pulverized coals involves the following key elements: 1) an effective multidisciplined means of characterizing the original coal for its inorganic content; 2) a controlled, small-scale combustion regime that can be quickly and easily manipulated to simulate the time and temperature profile in a full scale utility boiler; and 3) an effective means of characterizing the combustion products, such as fly ash generated in the small scale combustor. The abudance and mode of occurrence of inorganic components in coal are quantified using a combination of computer controlled scanning electron spectroscopy (CCSEM) and chemical fractionation techniques[1,2,3,4]. The CCSEM is used to determine the size and abundance of mineral grains in the coals. Chemical fractionation is used to quantify the abundance of organically associated elements. Ash is produced under carefully controlled combustion conditions using an entrained flow reaction or drop tube furnace system which simulates full scale utility boiler regimes[5,6,7,8]. The resulting ash is collected in a multicyclone which size-classifies the ash. The size segregated ash is characterized using a scanning electron microscope.

There are many methods of ash deposit and fly ash characterization which greatly enhance the ability of researchers to determine, with reasonable accuracy, the size distribution and composition of fly ash[9,10,11,12]. This allows for inferences to be made concerning the crucial factors involved in the transformation of inorganic components and also allows for the direct comparison of original mineral material with fly ash. In this particular study the mechanisms of coal ash formation were investigated for Monticello lignite from Titus County, Texas. The Monticello lignite was carefully prepared, analyzed, and combusted. The resulting ash was analyzed and compared to the original inorganic components in the coal.

EXPERIMENTAL

Coal Characterization

Monticello coal was characterized using a variety of analytical techniques. Standard ASTM coal and coal ash analyses were performed. Chemical fractionation[4] and computer-controlled scanning electron microscopy (CCSEM)[6,8]

were used to ascertain abundance and distribution of inorganic components, as well as the size and type of mineral grains in the coal.

Chemical fractionation was used to selectively extract elements from the coal based on solubility, which reflects their association in the coal. Briefly, the technique involves extracting the coal with water to remove water-soluble elements. This is followed by extraction with 1M ammonium acetate to remove elements that are associated as salts of organic acids. The residue of ammonium acetate extraction is then extracted with 1M HCl to remove acid-soluble species in the form of hydroxides, oxides, carbonates, and organically coordinated species. The components which remain in the residue after all three extractions are assumed to be associated with the insoluble mineral species such as clays, quartz, and pyrite.

The CCSEM analysis was performed on a 53-74μm sized fraction of Monticello lignite. Approximately 1000 mineral grains were type-classified based on elemental compositions, and sized according to average diameter. The size categorization of the grains was selected to be consistent with multicyclone cutpoints used in size-classifying the fly ash produced from this same coal fraction in the drop tube furnace. The CCSEM technique tends to underestimate the true average diameters of the mineral grains. Since the coal sample that is analyzed is a cross-section, the mineral grains observed are also cross-sectioned. This means that a mineral that has been sliced exactly at its average diameter is rare. To verify the CCSEM sizing technique, the coal minerals were also sized using a coulter counter analysis of a low temperature ash sample.

Fly Ash Production and Characterization

Fly ash was produced using an entrained-flow tube furnace, also known as a drop-tube furnace. The drop-tube furnace is a laboratory scale furnace system that has the ability to mimic conditions of commercial combustors without the high cost associated with pilot-scale combustion testing. The combustion temperature, residence time, and gas cooling rate can be closely controlled and monitored. Table 1 gives the combustion parameters used to produce the ash. More specific details of the EMRC drop-tube furnace are described elsewhere[13]). Fly ash was cooled by means of a fly ash quenching probe and collected using a multicyclone. The multicyclone aerodynamically separates the fly ash into 6 stages or aerodynamic categories. Each of the fly ash samples collected from the 6 stages was mounted in a suitable SEM mount and characterized using scanning electron microscopy and electron microprobe analysis. A technique called scanning electron microscopy point (SEMPC), which was developed at the EMRC, was employed to determine the relative abundance of phases present in the fly ash particles. The types of phases identified include: (1) phases that resemble the original components in the coal, (2) phases that have molar and weight ratios of elements that are consistent with known crystalline species, and (3) unclassified species that do not fit in the first two categories. This information is used to compare not only the compositional changes in the ash, but also the changes in phases as a function of particle size. Specific information regarding the SEMPC technique can be found elsewhere[10].

RESULTS AND DISCUSSION

Coal Characterization

The chemical fractionation results for the Monticello coal are found in Table 2. The large percentage of aluminum, silicon, potassium, and titanium remaining after the extraction implies that these elements were mostly associated with insoluble minerals as clays, quartz, and possibly rutile (titanium oxide). The results suggest that significant amounts of the alkali and alkaline earth elements are associated in the coal as salts of organic acid groups. For example, most of the magnesium, calcium, and strontium were removed by the ammonium acetate extraction. Potassium appears to be associated with a clay mineral. The iron was distributed as roughly half acid-insoluble sulfides (probably pyrite) and half organically coordinated or acid soluble minerals.

The Monticello coal has a relatively high ash content of 15%. From the chemical fractionation analysis it was calculated that at least 77.8% of the ash or 11.7% of the coal consisted of discrete mineral phases. Table 3 shows the distribution of discrete mineral phases in the Monticello 53-74μm coal, as determined by CCSEM. Nine minerals were observed in this size fraction of Monticello coal including: quartz, kaolinite, Fe-aluminosilicate, K-aluminosilicate, Ca-aluminosilicate, iron oxide, pyrite, rutile, and an aluminosilicate-gypsum mixture. The Fe and Ca-aluminosilicates were probably a type of montmorillonite and the K-aluminosilicate was most likely illite. One limitation of the CCSEM technique is that it is difficult to accurately classify clay minerals, except for kaolinite and in some instances, illite. Quartz was the most abundant mineral and was the dominant phase in all of the size ranges except for the >8.0-11.0μm range where kaolinite was the major phase. Figure 1 shows the abundance of five important mineral types observed in the six size categories. Quartz and Ca-aluminosilicate (montmorillonite) show approximately 70% of their mass in the >11μm size range. All five minerals shown in Figure 1 have a slight increase in content in the 2.1-4.4μm size range. Kaolinite is evenly distributed in a 1.2-11.0μm size range.

Fly Ash Characterization

The results of the SEMPC analyses are listed Table 4. Hauyne, which is a sodium - calcium aluminosilicate with sulfur, was observed in all of the samples except the 2.1-4.4μm range. The highest content of hauyne was observed in the 1.2-2.1μm range. Calcium oxide (which refers to species such as $CaCO_3$ and CaO), montmorillonite-derived material, illite, and iron oxide were detected only in small amounts in all stages. All size categories contained significant quantities of kaolinite-derived materials with the highest level found in the 1.2-2.1μm range. Anhydrite was relatively enriched in the 8.0-11.0μm size fraction and on the final filter. Plagioclase in the form of solid solution phases between end members albite ($NaAlSiO_4$) and anorthite ($CaAl_2Si_2O_8$), was observed at low levels, with none observed in the sample from the 4.4-8.0 μm size categories. The quartz content of the samples varied markedly between size categories. In the >11μm and 4.4-8.0μm size fractions, 25.4 and 31.8% quartz were detected, respectively. Melilite was present in all of the multicyclone stages except for the 2.1-4.4μm size range. The sample from the 4.4-8.0μm size category had the greatest number of unidentified phases (45.5%), whereas the 8.0-11.0μm and 2.1-4.4μm size ranges had the fewest unidentified phases (63.5 and 65.4%, respectively).

The chemical compositions (on an SO_3-free basis) of each sample are listed in Table 4 along with the Si/Al molar ratio. The most striking result shown in Table 4 was the high level of Mg and Fe in the ash collected on the final filter. The very high Fe and Mg contents in the final filter suggests they may have vaporized and subsequently condensed to form submicron size particles, or that they were organically associated which can also produce very small particles during combustion. The chemical fractionation results suggest that approximately 53% of the iron is associated organically and/or as a carbonate mineral. The CCSEM data shows that a very low level of iron was observed in the form of iron oxide/carbonate minerals. In addition, no significant amount of pyrite was found.

The Si/Al molar ratios did not indicate any apparent trends between the multicyclone samples. The 4.4-8.0 size range had the highest value while the 1.2-2.1μm range had the lowest. The data indicated that the >11μm, 4.4-8.0μm ranges were relatively enriched with silica (presumably quartz), whereas the 8.0-11.0μm and 1.2-2.1μm ranges were relatively depleted in silica.

The particle size distributions of the Monticello coal minerals, fly ash, and low temperature ash (LTA), as determined by CCSEM, multicyclone, and coulter counter analysis respectively, are shown in Figure 2. In all cases the majority of the mass was present in the larger size ranges. The minerals as determined by CCSEM show a bimodal distribution concentrated at the 2.1-4.4μm and >11 μm ranges. The CCSEM technique tends to underestimate the average diameter of mineral grains in cross-section. The LTA distribution shows nearly the same amount of material at the 2.1-4.4μm range as the CCSEM distribution, however, it has more particles with sizes in the 4.4-11.0μm range and less particles in the >11μm range. Two possible explanations for the differences between the LTA and CCSEM distributions are: 1) clay aggregates, which may be counted as only one particle in the CCSEM analysis, are usually broken up into smaller particles during the low temperature ashing process and 2) the LTA samples include mass from organically bound elements which are not quantified by CCSEM.

Figure 2 also shows that the fly ash distribution has very little mass in the lower size categories, but most of the particles are >11μm. This is evidence for the process of coalescence and expansion whereby variously sized minerals and organically bound inorganics in a coal particle coalesces to form a larger fly ash particle. Further expansion may be due to the escape of gaseous or volatile matter.

Comparisons were made between the content of selected minerals in the original coal and their corresponding phases in the fly ash on a percent mass basis. The Monticello coal ash concentration was determined to be 15% on a dry basis. From the chemical fractionation analysis it was calculated that at least 78% of the ash or 12% of the coal consisted of true mineral phases (referred to as mineral matter here). When comparing the percentage of coal mineral phases to the inorganic phases present in the fly ash it must be remembered that the fly ash consists of both organically bound elements and mineral matter. The CCSEM analysis of coal minerals does not include the minute, organically bound inorganics. Therefore, to compare the coal mineral and fly ash data, the mineral data was multiplied by a correction factor of 0.78 to evenly weight the comparisons. The limits of experimental error for this comparison procedure are approximately 10-20%.

Comparison of the percent kaolinite in the coal to the percent kaolinite-derived in the fly ash revealed that the concentrations for corresponding size ranges were within 15% of each other except for the 8.0-11.0μm range (Figure 3). Kaolinite in the coal had lower concentration than the kaolinite-derived in the fly ash, excluding the <1.2μm and 8.0-11.0μm ranges. This suggests that a large percentage of the finer grained kaolinite in the coal collects extraneous inorganic matter during combustion which thereby increases its mass to a higher value than what was seen in the original coal. Sodium, magnesium, and calcium, most likely from organically bound cations, were the primary additions to the kaolinite-derived mass. The distribution of quartz, as shown in Figure 4, revealed a higher percentage of quartz in the coal than in the fly ash for all size ranges. Both curves have the same trends of slope when lines are drawn between the size ranges.

CONCLUSIONS

The Monticello 53-74μm coal and its corresponding drop tube furnace fly ash were characterized for their inorganic matter as a means of better understanding the inorganic transformations involved. The Monticello coal had a high ash content of 15% and approximately 78% of the inorganic constituents were determined to be mineral grains. The major mineral types identified included quartz, kaolinite, and Ca-aluminosilicate (montmorillonite). Major organically bound elements included sodium, magnesium, calcium, strontium, and barium. Iron content in the Monticello coal consisted of roughly half insoluble sulfides (pyrite) and half organically-coordinated or other acid soluble species. Although the CCSEM technique provides valuable data concerning the size and distribution of mineral phases, in its current stage of development the CCSEM technique appears to underestimate the total mass of minerals present. The CCSEM technique is best applied along with chemical fractionation; the combination of these two techniques provides a very complete picture of the form and nature of inorganic constituents present in a low-rank coal.

The particle size distribution of the Monticello minerals, as determined by CCSEM, had a bimodal distribution with over 60% of its mass >11μm. The LTA distribution had only 33% of its mass >11μm. The differences between the LTA and CCSEM distributions may be due to the breakup of clay aggregates during the low temperature ashing or the exclusion of organically bound elements in the CCSEM analysis. The size distribution of the fly ash showed 90.9% of its mass >11μm. Apparently, smaller mineral grains and organically bound inorganics are agglomerating or being assimilated into the melt phase of other material during combustion.

Analysis of the 6 multicyclone size fractions of fly ash using SEMPC identified 13 types of inorganic phases. The most abundant phases observed were hauyne, kaolinite, anhydrite, plagioclase, quartz, melilite, and unclassified material. Hauyne, a complex aluminosilicate containing sulfate, was mostly concentrated in the smaller size fractions. Kaolinite-derived phases had a fairly uniform distribution in all of the size ranges except for an anomalously low value in the final filter. The majority of the anhydrite was found in the final filter fraction probably due to deposition as gaseous or very fine particulate matter. Quartz content varied markedly between size ranges. Higher levels of Mg and Fe were noted in the smallest size fraction (<1.2μm). These values may be a result of how the Mg and Fe was associated in the coal; as a significant portion of both Mg and Fe are associated with the

organic fraction of the coal. Therefore, the relative sizes of the resulting ash particles containing these elements may be limited to a finer size fraction.

In comparing coal minerals to fly ash minerals and phases on a percent mass basis, several trends were noted. A large percentage of the finer-grained kaolinite in the coal appears to have combined with other minerals or extraneous inorganics during combustion. This was evidenced by the increase of non-crystalline kaolinite (kaolinite-derived) in the fly ash as compared to the original coal.

ACKNOWLEDGEMENTS

This work was performed under contract to the Department of Energy under the Cooperative Agreement No. DE-FC21-86MC-10637. The authors thank the Contracting Officers Technical Representative, Mr. Philip M. Goldberg, for permission to publish the results.

REFERENCES

1. Straszheim, W.E., Yousling, J.G., Younkin, K.A., and Markuszewski, R., 1988, Mineralogical characterization of lower rank coals by SEM-based automated image analysis and energy - dispersive x-ray spectrometry: Fuel, v. 62, August, p. 1042-1047.

2. Benson, S.A. and Holm, P.L., 1985, Comparison of Inorganic Constituents in three low-rank coals: Ind. Eng. Chem. Prod. Res. Dev., 24, 145-149.

3. Huggins, F.E., Kosmack, D.A., Huffman, G.P., and Lee, R.J., 1980, Coal mineralogies by SEM automatic image analysis: Scanning Electron Microscopy, 1980, I, AMF O'Hare (Chicago), Illinois 60666, p. 531-540.

4. Russel, S.J. and Rimmer, S.M., 1979, Analysis of mineral matter in coal, coal gasification ash, and coal liquefaction residues by scanning electron microscopy and x-ray diffraction, in Karr, C., Jr., ed., Analytical Methods for Coal and Coal Products, v. III: Academic Press, p. 133-162.

5. Benson, S.A. and Austin, L.G., 1988, Study of slag deposit initiation using a laboratory-scale furnace: presented at the conference on mineral matter and ash deposition from coal, Engineering Foundation, Santa Barbara, California, February, 1988.

6. Sadakata, M., Mochizuki, H., Sakai, T., Okazaki, K., and Ono, M., 1988, Formation and behavior of submicron fly ash in pulverized coal combustion furnace: Combustion and Flame, v. 74, p. 71-80.

7. Abbot, M.F. and Austin, L.G., 1986, A study of slag deposit initiation in a drop-tube furnace: in Mineral Matter and Ash in Coal. Vorres, K.S., (ed.), ACS Symposium Series No. 301, Washington, D.C., p. 325.

8. Wibberley, L.J. and Wall, T.F., 1986, An investigation of factors affecting the physical characteristics of fly ash formed in a laboratory scale combustor: Combustion Science and Technology, v. 43, p. 177-190.

9. Furyua, K., Miyajima, Y., Chiba, T., and Kikuchi, T., 1987, Elemental Characterization of particle size - density separated coal fly ash by spetrophotometry, inductively coupled plasma emission spectrometry, and scanning electron microscopy - energy dispersive x-ray analysis: Environmental Science Technology, v. 21, no. 9, p. 898-903.

10. Kalmanovitch, D.P., Montgomery, G.G., and Steadman, E.N., 1987, Computer Controlled Scanning electron microscopic characterization of coal ash deposits: American Society of Mechanical Engineers, 87-JPGC-FACT-4, Presented at ASME/IEEE Power Generation Conference, Miami Beach, Florida - October 4-8, 1987.

11. Benson, S.A., Rindt, D.K., Montgomery, G.G., Sears, D.R., 1984, Microanalytical Characterization of North Dakota fly ash: Ind. Eng. Chem. Prod. Res. Dev., 23, p. 252-256.

12. Rothenberg, S.J., Denee, P., and Holloway, P., 1980, Coal Combustion fly ash characterization: electron spectrascopy for chemical analysis, energy dispersive x-ray analysis, and scanning electron microscopy: Applied Spectroscopy, v. 34, no. 5, p. 549-555.

13. Benson, S.A., Sweeny, P.G., Abrahamson, H.B., Radonovich, L.J., Zygarlicke, C.J., Puffe, W.H., and Maldonado, M.E., 1988, Combustion Inorganic Transformation -- Final Technical Report, DOE, April (1988).

TABLE 1

DROP-TUBE FURNACE RUN CONDITIONS

	Monticello
Particle Size	53-74 μm
Primary Air	1.25 L/min
Sec. Air	4 L/min
Vacuum	15 L/min
Quench Gas	3 L/min
Temperatures	
Preheat Injector	1000°C
Furnace 1	
In	1500°C
Out	1315°C
Furnace 2	
Mid-Point	1280°C
Residence time	sec.

TABLE 2

CHEMICAL FRACTIONATION RESULTS FOR MONTICELLO COAL

	Initial (μg/g dry coal)	% Removed by H_2O	% Removed by NH_4OAc	% Removed by HCl	% Remaining
Na	315	31	31	0	18
Mg	1180	0	70	4	26
Al	9110	0	0	5	95
Si	23600	0	0	1	99
K	335	21	5	0	74
Ca	7320	0	77	13	10
Ti	395	0	0	15	85
Fe	2200	0	0	53	47
Sr	130	0	72	11	17
Ba	100	0	52	26	22

TABLE 3

CCSEM MINERAL COMPOSITION OF MONTICELLO COAL
(Weight Percent of Total Discrete Minerals)

Mineral	Size Categories (micrometers)						Total %	Total Wt% Minerals
	<1.2	1.2-2.1	2.1-4.4	4.4-8.0	8.0-11.0	>11.0	Minerals	(Coal Basis)
Quartz	0.39	2.82	10.47	8.16	2.09	55.41	79.35	4.34
Kaolinite	0.11	0.61	2.13	1.6	2.65	0.0	7.09	0.39
Fe-Aluminosilicate	0.02	0.14	0.25	0.0	0.0	0.0	1.40	0.02
K-Aluminosilicate	0.03	0.27	1.26	1.05	0.0	0.0	3.04	0.17
Ca-Aluminosilicate	0.14	0.58	0.68	0.0	3.42	3.42	4.82	0.26
Iron Oxide/Carbonate	0.0	0.10	0.10	0.0	0.0	0.0	0.9	0.01
Rutile	0.03	0.12	0.32	0.0	0.0	0.0	0.48	0.03
Alum-Sili/Gypsum	0.03	0.13	0.07	0.37	0.0	2.73	3.34	0.18
Pyrite	0.0	0.06	0.07	0.0	0.0	0.0	0.13	0.01
Gypsum	0.0	0.0	0.0	0.0	0.0	0.0	0.0	0.00
Unknown	0.0	0.02	0.35	0.21	0.47	0.0	1.05	0.06
Coal								94.53
Total	2.75	4.89	15.77	11.40	5.63	61.56	100.0	100.00

TABLE 4

PHASES DETECTED BY SEMPC FOR MONTICELLO FLY ASH

	Filter	Stage 5	Stage 4	Stage 3	Stage 2	Stage 1
Particle Size Cutpoints (μm)	<1.2	1.2-2.1	2.1-4.4	4.4-8.0	8.0-11.0	>11.0
Percent Mass	2.0	2.4	1.1	1.6	2.0	90.9
Phase (Number %)						
Hauyne	1.6	11.2	1.0	0.0	2.9	0.5
Calcium Oxide	0.0	0.0	0.0	0.0	0.0	0.5
Montmorillonite +	0.0	0.7	1.0	0.0	0.0	1.5
Calcium Silicate	0.0	0.7	1.0	0.0	0.0	0.0
Illite	0.0	0.0	0.0	0.0	0.6	0.0
Iron Oxide	0.0	0.0	1.0	0.0	1.7	0.0
Kaolinite +	1.2	22.4	13.0	18.2	16.6	12.2
Anhydrite	28.0	1.4	0.0	2.3	6.3	0.5
Plagioclase	0.0	1.4	1.0	0.0	1.2	1.0
Quartz	0.0	2.1	16.3	31.8	6.3	25.4
Melilite	0.4	2.8	0.0	2.3	1.1	2.0
Pyroxene	0.8	0.0	0.0	0.0	0.0	0.0
Unclassified	67.9	56.6	65.4	45.5	63.5	56.3
Average Composition, wt% (SO_3-Free)						
SiO_2	29.5	37.7	51.5	51.7	43.5	64.0
Al_2O_3	10.2	18.2	15.2	11.6	17.5	15.1
Fe_2O_3	26.0	6.7	5.7	4.6	5.8	2.6
TiO_2	0.9	2.1	1.5	2.6	1.9	1.7
P_2O_5	0.2	0.3	0.5	0.4	0.4	0.5
CaO	15.8	27.4	19.9	23.1	23.7	12.6
MgO	16.0	5.6	3.7	4.0	4.6	2.3
Na_2O	1.1	1.6	1.7	1.6	2.0	0.8
K_2O	0.1	0.3	0.3	0.3	0.4	0.4
(SO_3)*	8.70	6.4	4.2	3.7	4.6	0.7
Average Si/Al Molar Ratio	2.5	1.8	2.9	3.8	2.1	3.6

*SO_3 added for comparison purposes.
+derived phases-resemble the original mineral in the coal.

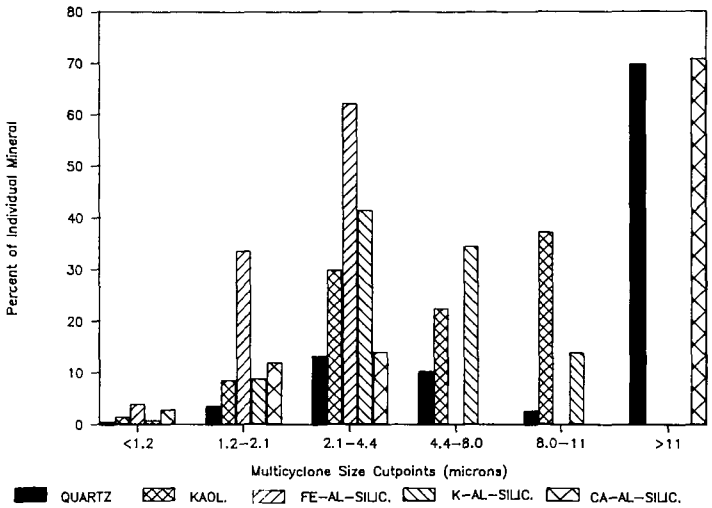

Figure 1. Size distribution of five individual mineral types in Monticello coal.

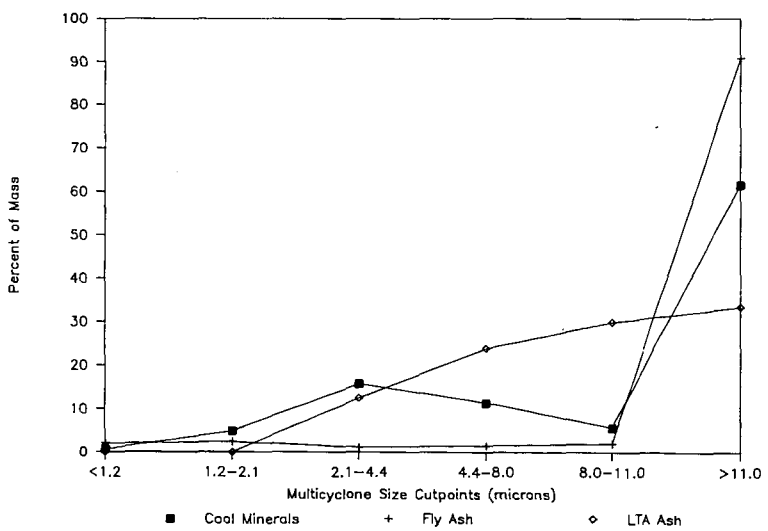

Figure 2. Particle size distribution of Monticello coal minerals, fly ash, and low temperature ash as determined by CCSEM, multicyclone, and coulter counter techniques, respectively.

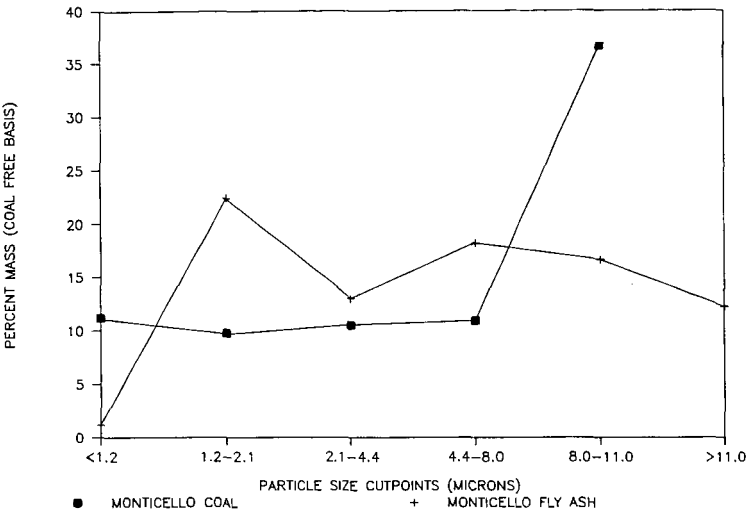

Figure 3. Distribution of Kaolinite in Monticello coal and Kaolinite-derived material in the Monticello Fly Ash.

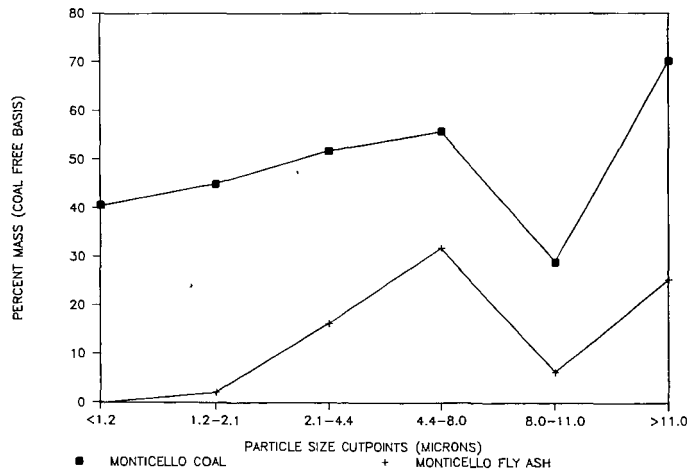

Figure 4. Distribution of Quartz in Monticello coal and Quartz-derived material in the Monticello Fly Ash.

BEHAVIOR OF BASIC ELEMENTS DURING COAL COMBUSTION

G. P. Huffman, F. E. Huggins, and Naresh Shah
CFFLS, University of Kentucky
233 Mining & Mineral Resource Building
Lexington, KY 40506-0107.

ABSTRACT

X-ray absorption fine structure (XAFS) spectroscopy, Mossbauer spectroscopy, and computer-controlled scanning electron microscopy (CCSEM) have been used to investigate the reactions of Ca, Fe, and alkalies in combustion systems. Ca may either transform to a CaO fume that reacts with SO_2 to form $CaSO_4$, or may react with clays, quartz, and other minerals to form slag droplets, or flyash. Similarly, pyrite may devolatilize and oxidize exothermically to form molten or partially molten iron sulfide-iron oxide mixtures, or may react with other minerals to become part of the slag. Alkalies in lignites (principally Na) volatize and may react with either SO_2 to form sulfates or with clay minerals (principally kaolinite) to form aluminosilicate slag droplets. K in bituminous coal is contained in illite which melts and becomes part of the slag phase. The calcium and alkali sulfates and the iron-rich species are observed to be concentrated in the initial layers of deposits, while the complex aluminosilicate slag droplets collect to form an outer glassy layer.

INTRODUCTION

The basic elements in coal ash (alkalies, Ca, Fe) exhibit an interesting dual behavior during combustion. Not surprisingly, this dual behavior is closely related to the way in which these elements are contained in the coal being burned. In this paper, some recent experimental results on the behavior of basic elements in combustion systems are reviewed and qualitative models of their combustion reactions are discussed.

EXPERIMENTAL PROCEDURES

Much of the data on which the current paper is based is summarized in detail in several recent and forthcoming publications.[1-7] Bituminous coals and lignites and a variety of combustion products obtained from both pilot scale combustion rigs and drop-tube furnaces have been investigated. The principal characterization techniques used were XAFS spectroscopy, Mossbauer spectroscopy, and computer-controlled scanning electron microscopy (CCSEM).

EXPERIMENTAL RESULTS

The principal experimental observations for the dominant basic elements are summarized below.

Calcium - In lignite, calcium is molecularly dispersed in the coal macerals and is bonded to the oxygen anions in carboxyl groups, while in bituminous coal it is predominantly contained in the discrete mineral, calcite. A systematic change from carboxyl-bound calcium to calcite is observed with increasing rank.[8] During pyrolysis and gasification reactions the molecularly dispersed calcium in lignite is observed to agglomerate and, eventually, form CaO.[1]

A recent XAFS study of the combustion products of a lignite and a bituminous coal detected two forms of Ca, Ca incorporated in aluminosilicate glass and $CaSO_4$[5]. Solids rapidly extracted from within and above the flame contained all Ca in glass. In both superheater and waterwall deposits, glass was the dominant Ca-bearing phase in the outer (fireside) deposits, while $CaSO_4$ was dominant in the inner or initial deposits. In work currently underway, the forms of Ca is samples produced by combustion of Beulah lignite and other coals in drop-tube furnace studies are being investigated by CCSEM and XAFS spectroscopy. Typical results are shown by the ternary diagram in Figure 1. Here each point represents an ash particle identified by the CCSEM analysis as containing >80% Ca + Si + Al. The composition of each particle, normalized to three elements, is then plotted on the ternary diagram. It is seen that there are a substantial number of Ca-rich (principally CaO) particles, and aluminosilicate glass particles with a fairly broad range of Ca contents.

Iron - Pyrite and its oxidation products are the dominant iron-bearing phases in both low and high rank coals, although bituminous coals frequently contain substantial amounts of iron in clays and siderite.[9] If pyrite is contained in a burning coal particle that also contains clay minerals and/or quartz, it is likely to react with these minerals to form an aluminosilicate slag droplet. Mossbauer spectroscopy has demonstrated that most of the iron in flyash samples quenched from within or above the flame of a pilot scale combustor, and most of the iron in the outer layers of deposits, is contained in aluminosilicate glass.[3,4]

Pyrite particles that are isolated within a coal particle or that are liberated behave much differently. Recently, Mossbauer spectroscopy and CCSEM measurements were conducted to determine the transformation products formed from pyrite removed from coal in drop tube furnace tests at gas temperatures of 1311 to 1727 K and residence times from 0.07 to 1.2 seconds in a 95% N_2 - 5% O_2 atmosphere.[6] Magnetite was the dominant oxide formed, while pyrrhotite ($Fe_{1-x}S$) was the dominant sulfide. CCSEM results show evidence of extensive melting, even at the lowest gas temperature. This is consistent with a thermodynamic model[10] which yields particle temperatures significantly in excess of the gas temperature because of the exothermic oxidation of pyrrhotite. These results are also consistent with the observation of iron-rich initial layers observed in deposits[3,4] that appear to have been formed from the impaction of highly viscous liquid droplets. The inner layer is

transformed to hematite over a period of time at the lower temperatures within the deposit near the waterwall or the superheater tubes.

Alkalies - The principal alkali species in lignite is Na, believed to be molecularly dispersed through the macerals and bonded to the oxygen anions in carboxyl groups. K is low in abundance but can be inserted into carboxyl bound sites in the coal macerals by cation exchange. In bituminous coals, K is the dominant alkali and it is contained almost exclusively in the clay mineral illite. Illite has a strikingly different XAFS spectrum from that of cation-exchanged K in lignite.[2] Na in bituminous coals is usually contained as NaCl, frequently in solution in moisture adsorbed in coal pores and capillaries.[11]

The behavior of alkalies during combustion is strongly dependent on their form in the coal. Carboxyl bound alkalies or alkalies in solution volatilize. Several volatile species are possible, but NaOH is the most likely for lignite.[12] K in illite is likely to remain with the aluminosilicate particle and form a molten slag droplet. Partial melting occurs at 900-1000°C because of eutectic regions in the K_2O - SiO_2 - Al_2O_3 phase diagram.[13,7] Volatile alkalies have a strong tendency to be absorbed by the aluminosilicates derived from clays[7,12] and significantly lower the melting point of the resulting slag. This is illustrated by Figure 2 which shows the ternary Na - Si - Al diagram generated from CCSEM data on ash particles collected during combustion of Beulah lignite in a drop-tube furnace. Each data point indicates the normalized three-element composition of a particle identified in the CCSEM analysis as containing $\geq$80% Na + Si + Al. The Ca - Si - Al diagram of Figure 1 is from the same sample. It is seen that the NaO_2 - SiO_2 - Al_2O_3 slag particles fall into a relatively small range of compositions.

When volatile alkalies reach the upper regions of the furnace they react with SO_2 to form molten alkali sulfates that react strongly with metal superheater tubes.[14] In a limited set of experiments, we have used XAFS and CCSEM to determine that superheater deposits from a boiler firing North Dakota lignite contained a mixture of alkali sulfate and alkali-containing glass.[15]

SUMMARY AND DISCUSSION

On the basis of the results summarized above, qualitative models of the behavior of the major basic elements during combustion can be deduced. These models are indicated in the schematic diagrams of Figure 3.

Calcium in lignite is molecularly dispersed and bonded to carboxyl groups in the macerals. It rapidly agglomerates into Ca - O clusters and CaO, while the calcite in bituminous coal devolatilizes to form CaO. The CaO may be given off from the burning coal particles as a CaO fume or may remain with the particles and react with the clay, quartz or other minerals to form a molten aluminosilicate slag. The CaO fume apparently reacts with SO_2 to form $CaSO_4$ which is part of the initial, presumably sticky, layer in both superheater and waterwall deposits[5].

Pyrite that is liberated or isolated alone in a coal particle devolatizes to form pyrrhotite which undergoes exothermic oxidation that raises the particle temperature sufficiently far above the gas temperature to exceed the melting point of magnetite.[6,10] The molten iron-rich particles impinging on the walls and tubes may be iron sulfide-iron oxide mixtures or magnetite, depending on residence time and temperature. Because of the high momentum of these particles, they readily impinge on the walls and tubes, forming a major part of the initial sticky layer for pyrite-rich coals. Those pyrite particles that are contained in coal particles containing clay, quartz and other minerals react to form molten aluminosilicate slag or flyash droplets which stick on top of the initial iron-rich, layer.

There is less good experimental data on alkalies in combustion systems. Nevertheless, some speculations can be made. It appears that Na is bound to carboxyl groups in lignite and readily volatilizes, presumably to NaOH, although other volatile species are certainly possible. Sodium reacts strongly with clay (mainly kaolinite in lignite) and quartz, both within the burning coal particle and in the vapor phase to form aluminosilicate slag droplets or flyash. The volatile NaOH also reacts with SO_2 to form $NaSO_4$ which has a low melting point (884°C) and becomes part of the initial sticky layer.

Finally, K in bituminous coal is contained in illite which melts and becomes part of the slag or flyash component of the ash stream.

While the simple diagrams of Figure 3 are consistent with the general trend of slagging and fouling behavior observed in coal combustion systems, it is clear that we have ignored many reactions and made a number of speculations for which there is no firm experimental proof. The current "model", therefore, should really be considered as a point of departure for future discussion and experimentation.

ACKNOWLEDGEMENT

This research was sponsored by the U.S. Department of Energy under DOE Contract No. DE-AC22-86PC90751.

REFERENCES

1. F. E. Huggins, N. Shah, G. P. Huffman, R. G. Jenkins, F. W. Lytle, and R. B. Greegor, Fuel, 67, 938-942 (1988).

2. G. P. Huffman, F. E. Huggins, and N. Shah, "EXAFS Spectroscopy: A New Technique for Investigating Impurity Elements in Coal that Control Slagging and Fouling Behavior," Engineering Foundation Conference on Mineral Matter and Ash in Coal, Santa Barbara, CA, 1988, Eds., K. S. Vorres and R. W. Bryers, to be published by Elsevier.

3. F. E. Huggins, G. P. Huffman, and A. A. Levasseur, "Ash Deposits from Raw and Washed Coals," ibid.

4. F. E. Huggins, G. P. Huffman, and A. A. Levasseur, ACS Division of Fuel

Chemistry Preprints, Vol. 33, No. 2, 73-80 (1988).

5. G. P. Huffman, F. E. Huggins, A. A. Levasseur, F. W. Lytle, and R. B. Greegor, "Investigation of the Atomic Structure of Calcium in Ash and Deposits Produced During the Combustion of Lignite and Bituminous Coal," Fuel, in press.

6. G. P. Huffman, F. E. Huggins, A. A. Levasseur, O. Chow, S. Srinivasachar, and A. Mehta, "Investigation of the Transformations of Pyrite in a Drop-Tube Furnace," Fuel, in press.

7. G. P. Huffman, F. E. Huggins, R. W. Shoenberger, J. S. Walker, F. W. Lytle, and R. B. Greegor, Fuel 65, 621-632 (1986).

8. G. P. Huffman and F. E. Huggins, in: Chemistry of Low-Rank Coals, ACS Symposium Series 264, Ed., H. H. Schobert, pp. 159-174, Amer. Chem. Soc., 1984.

9. G. P. Huffman and F. E. Huggins, Fuel 57, 592 (1978).

10. S. Srinivasachar and A. A. Boni, " A Kinetic Model for Pyrite Transformations in a Combustion Environment," Fuel, in press.

11. F. E. Huggins, G. P. Huffman, F. W. Lytle, and R. B. Greegor, "The Form of Occurrence of Chlorine in U. S. Coals: An XAFS Investigation," ACS Division of Fuel Chemistry Preprints, this volume.

12. L. J. Wibberly and T. F. Wall, Fouling and Slagging Resulting from Impurities in Combustion Gases, R. W. Bryers Ed., Engineering Foundation, New York, NY, 1983; pp. 493-513.

13. E. M. Levin, H. F. McMurdie and H. P. Hall, Phase Diagrams for Ceramists, Amer. Ceramic Soc., Inc., Columbus, Ohio, 1964.

14. W. T. Reid "Coal Ash--Its Effect on Combustion Systems," pp. 1389-1446, Chemistry of Coal Utilization, M. A. Elliott, Ed., J. Wiley, 1981.

15. G. P. Huffman and F. E. Huggins, "Reactions and Transformations of Coal Mineral Matter at Elevated Temperatures," Amer. Chem. Soc. Symposium on Mineral Matter/Ash in Coal, Philadelphia, PA, 1984; ACS Symposium Series No. 301, pp. 100-113, 1986.

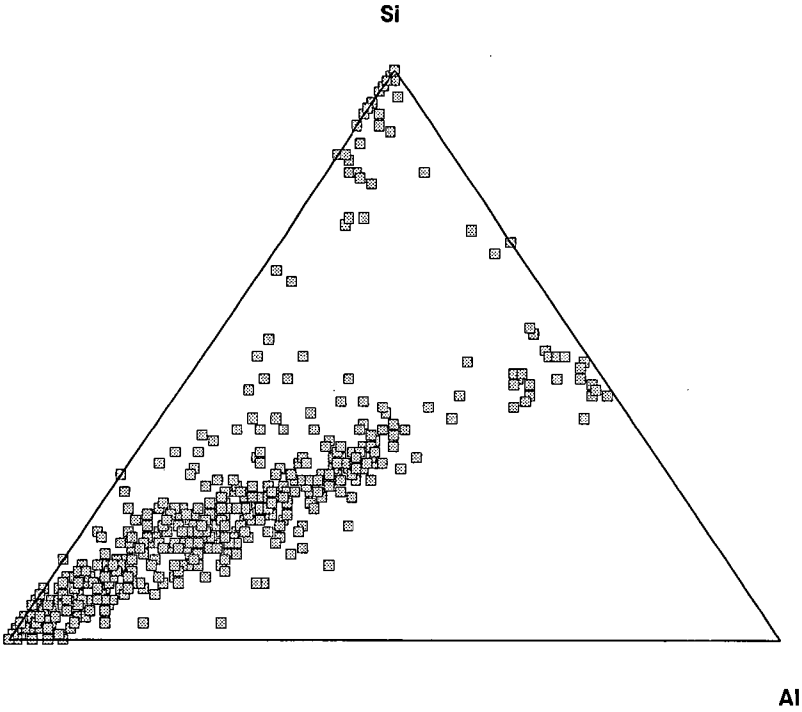

Figure 1. Ca - Si - Al diagram derived from CCSEM data for Beulah ash particles from a drop tube furnace combustion experiment.

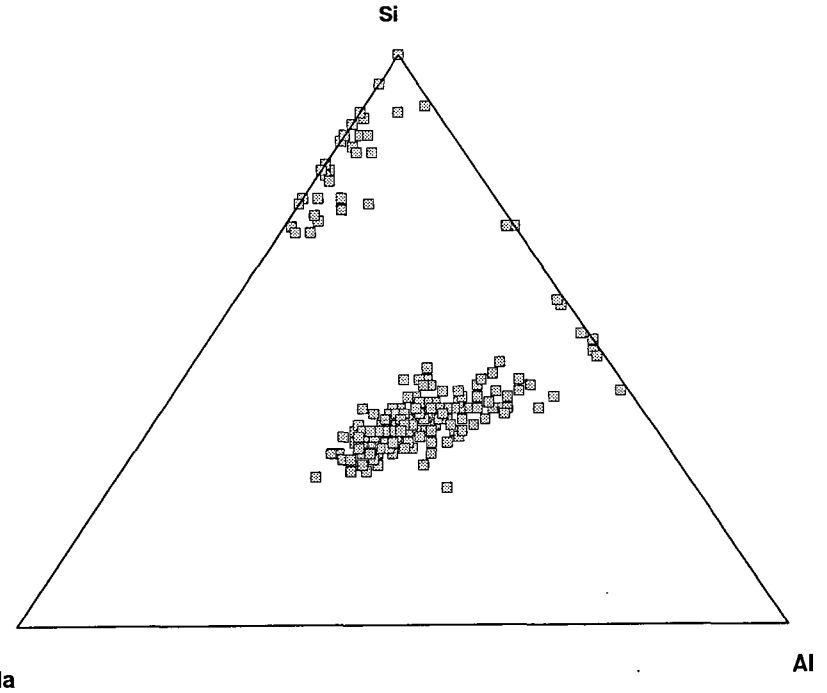

Figure 2. Na - Si - Al diagram derived from CCSEM data for Beulah ash particles from a drop tube furnace combustion experiment.

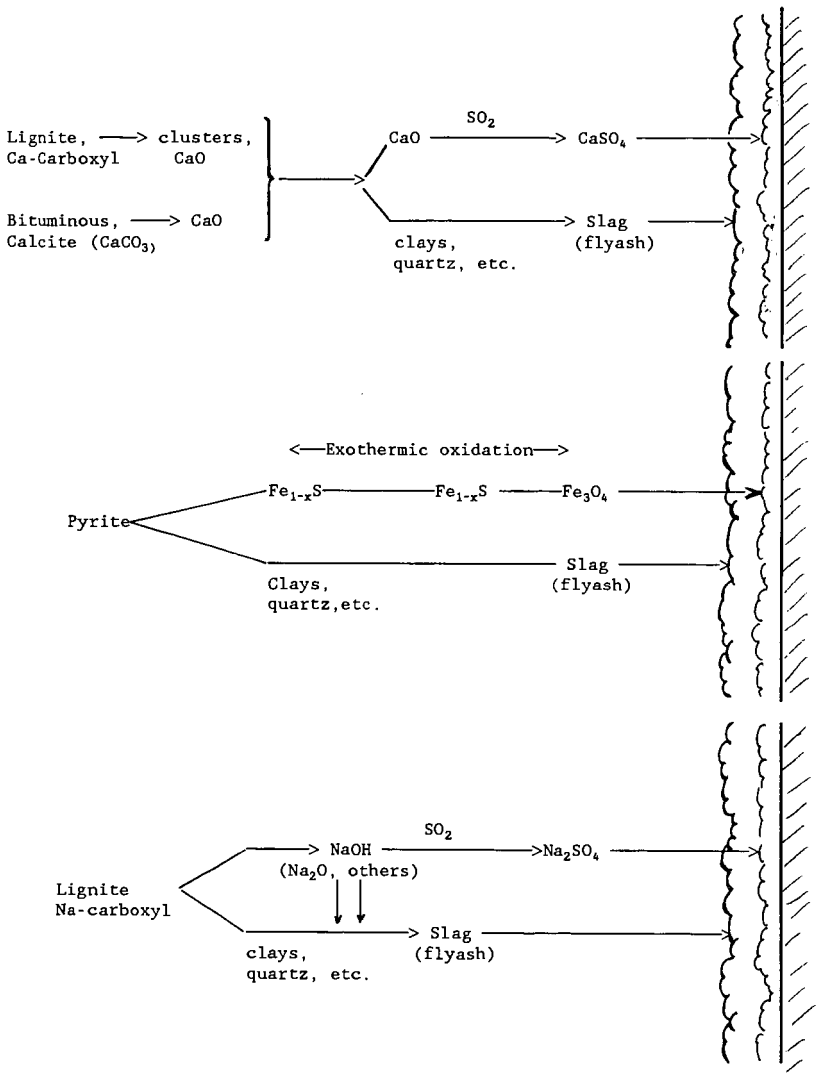

Figure 3. - Schematic diagram indicating the behavior of basic elements in combustion systems.

THE CHEMISTRY OF SODIUM WITH SULFUR IN FLAMES

Martin Steinberg and Keith Schofield
Quantum Institute
University of California
Santa Barbara, CA 93106

INTRODUCTION

The use of fuel/air systems contaminated with sodium and sulfur in combustion driven gas turbines is a source of turbine blade corrosion. Sodium sulfate, which deposits on turbine surfaces or is chemically formed there, has long been recognized as the active corrosive agent.[1,2] There is very little chemical kinetic information for modeling this practical problem, and one is forced to invoke chemical equilibrium to attempt any quantitative treatment.

Sodium/sulfur chemistry has been addressed in a very few studies. Fenimore[3] reported a decrease of Na with the addition of SO_2 to rich and lean H_2/Air flames which he attributed to the equilibration of Reaction (1).

$$NaOH + SO_2 = NaSO_2 + OH \qquad (1)$$

Durie et al[4], in a study in rich and lean $C_3H_8/O_2/N_2$ flames assigned the observed Na decay with sulfur addition to the equilibration of Reactions (2) and (3), respectively.

$$NaOH + S = NaS + OH \qquad (2)$$
$$NaOH + SO_3 = NaSO_3 + OH \qquad (3)$$

They also felt that Fenimore's data supported their model. In a mass spectrometric study in a lean CH_4/Air flame, Fryburg et al[5] identified $NaSO_2$, $NaSO_3$, and Na_2SO_4 as gas phase products in lean methane-oxygen flames. They reported clogging of their sampler inlet orifice which limited their data gathering. In fact, it is not possible to conclude whether the observed species are homogeneous gas phase products, or are formed heterogeneously in the sample inlet probe.

The present study is an outgrowth of two previous efforts in this laboratory, sulfur chemistry[6] and sodium oxidation chemistry[7], in $H_2/O_2/N_2$ flames. Sodium/sulfur chemistry competes with the sodium oxidation chemistry and both are influenced by the flame radical/sulfur chemistry interaction. A brief overview follows.

The radicals H, O, and OH in the hot burnt gases of $H_2/O_2/N_2$ flames sharply overshoot their equilibrium levels through rapid bimolecular chain Reactions (4-6)

$$H + O_2 = OH + O \qquad (4)$$
$$O + H_2 = OH + H \qquad (5)$$
$$H_2 + OH = H_2O + O \qquad (6)$$

which are balanced due to their large kinetic fluxes in an otherwise non-equilbrated environment. Thus from measures of OH and temperature the concentrations of H, O, OH, and O_2 in rich or H_2 in lean flames

are calculable. The radicals recombine through slow 3-body reactions. With the addition of sulfur to these flames, radical recombination is catalyzed and in turn the radicals establish balances between SO_2, SO, H_2S, SH, S_2, and S. As with the flame radicals, the concentrations of these sulfur species also can be determined from measures of OH and T and the total sulfur content. SO_3 is formed in the slow termolecular Reaction 7.

$$SO_2 + O + M = SO_3 + M \qquad (7)$$

It can be assumed to be in steady state through Reaction 7 followed by reactions of SO_3 with H and O regenerating SO_2.

The oxidation of sodium in lean, sulfur free, $H_2/O_2/N_2$ flames was found to exhibit an interesting chemistry.[7] The dominant oxidation path occurs through a fast 3-body process

$$Na + O_2 + M = NaO_2 + M \qquad (8)$$

and the NaO_2 then reacts with the radicals to produce overshoots in NaOH concentrations, which are balanced with small amounts of NaO. A kinetic model was developed for this system from which the concentration profiles of Na, NaO_2, NaOH, and Na are determined from measures of OH and T and the total sodium concentration. The sodium/sulfur interaction is imbedded in this complex but reasonably understood environment.

EXPERIMENTAL CONDITIONS

Measurements are made in the laminar, premixed, one dimensional flow in the post flame gases above a Padley-Sugden[8] burner of bundled hypodermic tubing with an overall diameter of 2.2 cm. Sodium is introduced as an aqueous $NaNO_3$ aerosol generated in an ultrasonic nebulizer[9] and transported by a portion of the gas flow to the burner. Sulfur is added as H_2S and SO_2 to rich and lean flames, respectively, to minimize thermal contributions these additives make to flame properties. A schematic of the optical system is shown in Figure 1. Temperatures are measured using the sodium line reversal method. Sodium and OH are measured by laser induced fluorescence[10,11] using a YAG pumped dye laser source beam passed through the flame parallel to the burner surface. The fluorescence, from a slice of the laser excited flame volume is collected by a 6 inch mirror, passed through an image rotator, and focused into the vertical entrance slit of the monochromator. The burner is mounted on a motor driven table programmmed to collect data as a function of distance (and time) above the burner surface. The monochromator output is detected with a photomultiplier, the signal amplified, processed in a boxcar integrator, and recorded.

One line of the sodium doublet at 589.0 nm was pumped with fluorescence detection at 589.6 nm. Saturation excitation was employed to eliminate quenching uncertainties. The $OH(A^2\Sigma^+ - X^2\Pi)$ (1,0), $R_1(6)$ transition was excited at 281.14 nm and fluorescence detected at 314.69 nm from the (1,1), $Q_1(7)$ transition. The OH measurements are absolute values calibrated against a high temperature flame in which OH is at thermodynamic equilibrium.[12]

RESULTS

Measurements of temperature, OH, and Na have been made in 10-lean and 9-rich $H_2/O_2/N_2$ flames containing sodium with and without added sulfur. The flame matrix is listed in Table 1. Measured (Na) and (OH) profiles are plotted for a lean flame in Figure 2. It should be noted that the decreases in (Na) with added SO_2 result from two effects. The first may be the formation of some Na/S compound. The second, which is dominant in lean flames, is the increased sodium oxidation resulting from the sulfur catalyzed flame radical decay. It is this interaction that complicates the analysis.

KINETIC MODELING

The sodium experimental data has been scaled to refer to the same amount of total sodium in each flame. Sodium concentrations are the order of 10^{11} cm^{-3}, the radicals at least a few orders of magnitude greater, with total sulfur at the 1 to 2% level. Thus all species can influence (Na) but sodium has no effect on other species concentrations.

Checks on the balanced chemistry of Reactions (1-3), suggested by Fenimore[3] and Durie et al[4], indicated no such equilibrations. Plots of log K against T^{-1} for each of the reactions did not correlate the data. Apparently the chemistry is more complicated, requiring kinetic modeling.

With no sulfur present, the total sodium concentration, $(Na)_T$, is given by Equation 9, and with sulfur by Equation 10.

$$(Na)_T = (Na)_o + (NaO_2)_o + (NaOH)_o + (NaO)_o \quad (9)$$

$$(Na)_T = (Na)_s + (NaO_2)_s + (NaOH)_s + (NaO)_s + (NaX) \quad (10)$$

The subscript "s" indicates the presence of sulfur and (NaX) is a sodium/sulfur compound. To begin the analysis we will assume the formation of a single, dominant NaX. Eliminating $(Na)_T$ we obtain Equation (11)

$$(Na)_s = \frac{(1 + x + y + z)_o}{(1 + x + y + z + w)_s} (Na)_o \quad (11)$$

where $x = (NaO_2)/(Na)$, $y = (NaOH)/(Na)$, $z = (NaO)/(Na)$, and $w = (NaX)/(Na)$. Equation (11) relates the sodium concentrations with and without sulfur at corresponding times in the profiles for a given flame. The parameter $(1 + x + y + z)_o$ is calculated using the oxidation model for the sulfur free flames. We have used Equation (11) to calculate the values for $(Na)_s$ from the experimental values for corresponding $(Na)_o$ in the sulfur free flames. The parameter $(1 + x + y + z + w)_s$ is modeled to achieve a comparison between the so calculated $(Na)_s$ values and those observed experimentally.

A list of possible reactions have been written for the production and consumption of NaSO, $NaSO_2$, $NaSO_3$, NaSH, NaS, and NaS_2. At the sodium levels in this study there is little chance for the formation of any disodium compounds, such as Na_2SO_4. Vibrational frequencies

and bond lengths have been estimated for calculating thermodynamic properties of the sodium/sulfur species.[13] Estimates have been made for the gas kinetic collision rates of all the bimolecular reactions. Forward and reverse rate constants, related through the calculated equilibrium constants, have been formulated with the dissociation energy, D_0(NaX), for each of the assumed NaX products, as a parameter to be determined in the modeling program.

(NaO_2), (NaOH), (NaO), and (NaX) in the sulfur bearing flames were determined using a steady state analysis for these species. Three body rate constants for sodium with sulfur species were set initially equal to the rate constants for the sodium-oxygen analogs. Values for D_0(Na-X) and attenuating multipliers for each rate constant were then adjusted to achieve an optimal fit between calculated and experimental values for $(Na)_s$.

A reaction scheme for NaSO, added to the sodium oxidation model is seen in Figure 3. A comparison of the calculated and experimental profiles for $(Na)_s$ are plotted in Figure 4. The optimal conditions required only reactions (21), (23), and (24) from Figure 3. All the remaining sodium/sulfur processes have negligible influence. NaSO and NaO_2 are isoelectronic and it was assumed that the termolecular formation rate constants for NaSO and NaO_2 are equal. The model yielded a value for D_0(Na-SO) = 70 kcal/mole. NaSO concentrations varied from about 1 to 24% of the total sodium in the rich flames with lower temperatures favoring the higher concentrations. NaOH concentrations ranged from about 1 to 16% with the higher concentrations favored in the high temperature flames. There appears to be little coupling of the sodium sulfidation and oxidation chemistries. Application of the NaSO model to the lean $H_2/O_2/N_2$ flames only made a small contribution to that chemistry.

Similar analyses have been conducted in the rich flames assuming NaS, NaS_2, and NaSH as the primary sodium/sulfur product. NaS modeling does not quite approach the performance of the NaSO model. In addition the NaS optimal conditions require a value for D_0(Na-SO) = 81 kcal/mole, about 25 kcal/mole too large, ruling out NaS as a dominant product. NaSH and NaS_2 exhibit poorer accommodations to the experimental data.

Only $NaSO_2$ and $NaSO_3$ are possible candidates in the lean flames. $NaSO_3$ was ruled out as a meaningful product primarily due to the very low SO_3 steady state concentrations. $NaSO_2$ has been examined as a dominant product in both the rich and lean flames. Optimal rich flame conditions for $NaSO_2$ required D_0(Na-SO) = 70 kcal/mole. When applied to the lean flames this model consumed far too much sodium. Modeling $NaSO_2$ in the lean flames gave a very good approximation to the experimental data with a value for D_0(Na-SO) = 46 kcal/mole. The application to the lean flame data in Figure 2 is seen in Figure 5. In the lean flames $NaSO_2$ levels reach a maximum of only about 0.5% of the total sodium. The higher values are favored in the richer and cooler flames. NaOH accounts for 8 to 70% of the total sodium with higher values in the leaner flames. It does appear, however, that there is some increased NaOH formation occuring through the small but effective $NaSO_2$ intermediate. In the rich flame this $NaSO_2$ model makes a small, almost negligible contribution.

CONCLUSIONS

The sodium/sulfur chemistry has been modeled in a series of rich and lean $H_2/O_2/N_2$ flames. It was found that simple equilibria identified in earlier studies can not account for the behavior exhibited in the present data. Kinetic modeling has been conducted assuming, as is often the case, that one sodium/sulfur product may dominate. To a good approximation this seems to be the situation in both the rich and lean flames. NaSO appears to be the dominant sodium/sulfur product in the rich $H_2/O_2/N_2$ flames with $NaSO_2$ dominant in the lean flames.

The conclusions drawn for the lean flames are fairly firm. $NaSO_2$ is the only viable sodium/sulfur product in this oxidizing environment. However, we must view the rich flame discussion as provisional. It is possible that some combination of NaSO with $NaSO_2$, or even NaS or NaSH can provide a better description of the rich flame behavior. Currently, these combinations of contributing sodium/sulfur products are being examined.

ACKNOWLEDGEMENT

The support of this work by the Department of Energy, Morgantown Energy Technology Center under Grant DE-FG21-86MC23135 is gratefully acknowledged.

REFERENCES

1. E.L. Simons, G.V. Browning, and H.A. Liebhafsky, Corrosion, 11, 505t (1955).
2. M.A. DeCrescente and N.S. Bornstein, Corrosion, 24, 127 (1968).
3. C.P. Fenimore, Symp. (Int.) on Combustion, 14, 955 (1973).
4. R.A. Durie, G.M. Johnson, and M.Y. Smith, Symp. (Int.) on Combustion, 15, 1123 (1975).
5. G.C. Fryburg, R.A. Miller, C.A. Stearns, and F.J. Kohl, in "High Temperature Metal Halide Chemistry," D.L. Hildenbrand and D.D. Cubicciotti, Editors, p. 468, The Electrochemical Society Softbound Proceedings Volume 78-1, Princeton, NJ (1978); also NASA TM-73794 (1977).
6. C.H. Muller, K. Schofield, M. Steinberg, and H.P. Broida, Symp. (Int.) on Combustion, 17, 867, (1979).
7. J.T. Hynes, M. Steinberg, and K. Schofield, J. Chem. Phys. 80, 2585 (1984).
8. P.J. Padley and T.M. Sugden, Proc. Roy. Soc. London Ser. A, 248, 248 (1958).
9. M.B. Denton and D.B. Swartz, Rev. Sci. Instrum. 45, 81 (1974).
10. K. Schofield and M. Steinberg, Opt. Eng. 20, 501 (1981).
11. J.T. Hynes, M. Steinberg, and K. Schofield, J. Chem. Phys. 80, 2585 (1984).
12. C.H. Muller III, K. Schofield, and M. Steinberg, ACS Symp. Series, 134, 103 (1980).
13. B.J. McBride and S. Gordon, "Fortran IV Program for Calculation of Thermodynamic Data," NASA TN D-4097, August, 1967 (Updated version).

Table 1. Experimental Hydrogen/Oxygen/Nitrogen Flame Matrix and Properties.

$H_2/O_2/N_2$	Temperature (K)	$[H_2O]$	$[O_2]$	$[H_2]$	[OH]
			(molecules/cm^3)		
0.6/1/1	1906-1929	1.0(18)	1.2(18)	---	3.8->0.7(16)[a]
1/1/2	2066-2100	9.9(17)	4.8(17)	---	3.8->1.1(16)
1/1/3	1667-1730	9.5(17)	4.7(17)	---	3.7->0.3(16)
1.4/1/3	2125-2197	9.8(17)	2.0(17)	---	3.5->1.4(16)
1.4/1/4	1810-1847	9.8(17)	2.1(17)	---	3.6->0.5(16)
1.4/1/5	1654-1669	9.3(17)	2.0(17)	---	3.6->0.3(16)
1.8/1/3	2280-2405	1.1(18)	5.9(16)	---	4.0->1.9(16)
1.8/1/4	2060-2228	9.8(17)	5.1(16)	---	3.6->1.4(16)
1.8/1/5	1825-1916	1.0(18)	5.3(16)	---	3.2->0.7(16)
1.8/1/6	1695-1726	9.6(17)	5.2(16)	---	3.1->0.4(16)
2.2/1/4	2160-2308	1.0(18)	---	1.1(17)	3.8->1.3(16)
2.2/1/5	1975-2106	9.7(17)	---	9.8(16)	2.7->0.8(16)
2.2/1/6	1780-1897	9.4(17)	---	9.4(16)	1.9->0.5(16)
3/1/4	2050-2167	9.7(17)	---	5.5(17)	2.4->0.3(16)
3/1/5	1883-2010	9.1(17)	---	4.6(17)	1.2->0.2(16)
3/1/6	1775-1857	8.8(17)	---	4.4(17)	1.1->0.2(16)
4/1/4	1898-2042	9.1(17)	---	9.1(17)	1.0->0.2(16)
4/1/5	1767-1900	8.6(17)	---	8.7(17)	0.6->0.1(16)
4/1/6	1650-1788	8.2(17)	---	8.2(17)	0.6->0.1(16)

[a]Concentrations, read as 3.8×10^{16} near the flame reaction zone decaying downstream to 0.7×10^{16} at 4.0 ms.

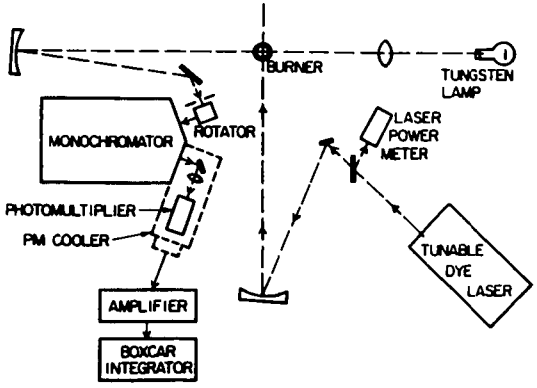

Figure 1. Optical Arrangement

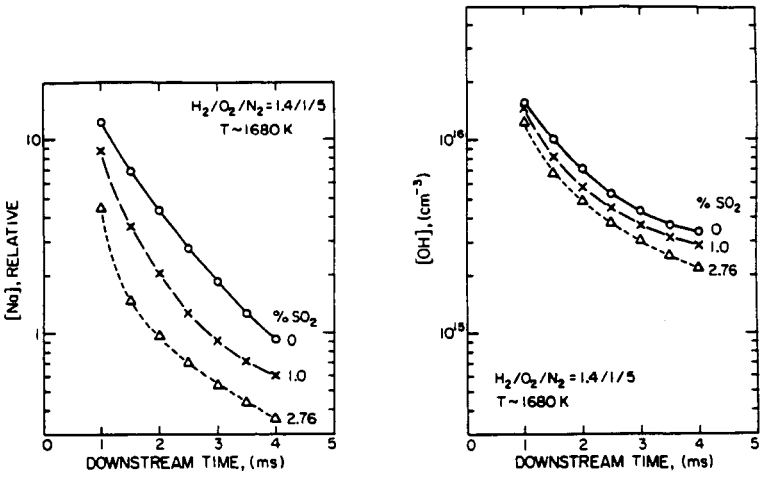

Figure 2. Measured (Na) and (OH) profiles in lean $H_2/O_2/N_2$ flames with varying amounts of SO_2.

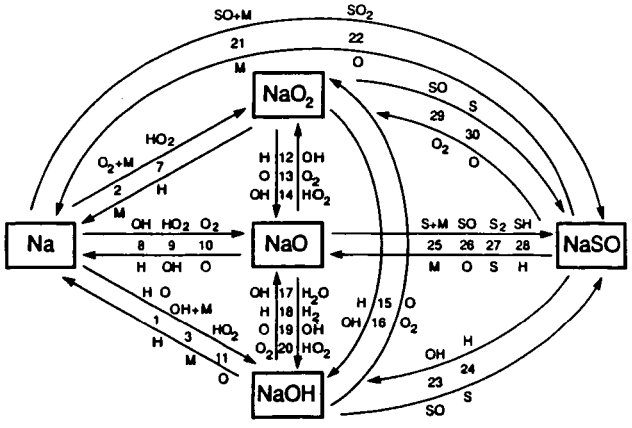

Figure 3. Sodium/sulfur reaction scheme assuming that NaSO is the dominant sodium/sulfur product.

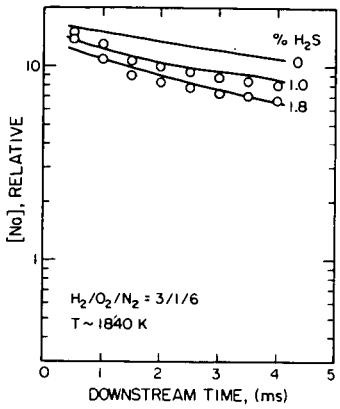

Figure 4. Comparison of measured and calculated sodium profiles in rich $H_2/O_2/N_2$ flames with varying H_2S and NaSO the dominant sodium/sulfur product. Measured, ————; calculated, O.

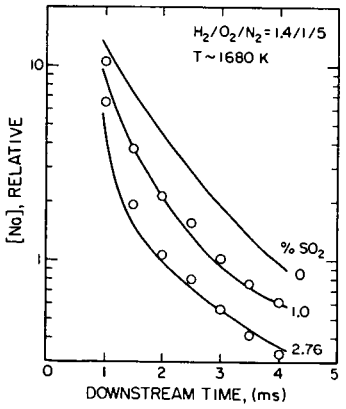

Figure 5. Comparison of measured and calculated sodium profiles in lean $H_2/O_2/N_2$ flames with varying SO_2 and $NaSO_2$ the dominant sodium/sulfur product. Measured, ————; calculated, O.

MINERAL TRANSFORMATIONS IN SELECTED COALS - SIZE AND COMPOSITION OF THE ASH

J.J. Helble, S. Srinivasachar, C.B. Katz, and A.A. Boni
PSI Technology Company
Research Park P.O. Box 3100
Andover MA 01810

ABSTRACT

The transformation of minerals during pulverized coal combustion has been examined by burning utility sized coals (70% < 200 mesh) in a laboratory-scale combustor. Experiments were conducted with several coals possessing different mineralogies, with particular attention paid to Kentucky #11 bituminous. Size and composition of the initial minerals and the resulting ash were measured by a variety of techniques, including computer controlled SEM, low temperature ashing, deposition on a cascade impactor, and optical (Malvern) particle size analysis. Results for the Kentucky #11 coal suggest a large degree of coalescence is occurring between illite, kaolinite, and quartz minerals, with occasional iron incorporation into the resulting glass. Partitioning of the acid-leachable potassium was found to split between incorporation into the glass and vaporization. For other coals, such as Beulah lignite, mineral fragmentation was inferred from the data, presumably due to large quantities of large (>40 microns) pyrite present.

BACKGROUND

Deposition of ash on heat transfer surfaces is the most costly problem associated with the combustion of pulverized coal. Although much research is currently focused toward obtaining a better understanding of the factors giving rise to deposition, current industry practice is to address the problem in an empirical manner which often proves unsatisfactory and inaccurate (1). In determining deposition indices, ash is treated as a homogeneous medium, possessing uniform properties. This neglects the fact that combustion generated ash is actually comprised of individual particles, of a wide variety of sizes and compositions. By treating the ash as disparate particles rather than as a homogeneous medium, it is possible that better deposition indices could be developed.

There are several components which must be addressed in determining the deposition behavior of an ash particle, and by extension, of a particular coal. Size, chemical composition and adhesive properties of the surface layers (i.e. stickiness) are all important considerations. The stickiness of ash particles has been addressed elsewhere (2,3); preliminary results of an experimental study of the factors giving rise to the observed size and composition distributions of ash are discussed herein. Several recent laboratory studies have utilized the size of the ash particles to infer the importance of various phenomena such as fragmentation, fines carry-over, and coalescence (4-9). Utilization of size information coupled with mineral and

ash compositional information for a particular coal to provide an overall picture of the important processes, is the focus of this study. Several U.S. coals and one Australian coal are being examined, with the results from one particular coal - Kentucky #11 bituminous - highlighted.

EXPERIMENTAL APPROACH

Combustion experiments were conducted in a laboratory scale drop-tube combustor which incorporates a gas-fired swirl-stabilized section on the front end to increase residence time and simulate particle concentrations present in an actual combustor. Details of this system are provided elsewhere (2). Ash particles were sampled isokinetically, quenched, and collected with a variety of techniques depending upon the desired information. Size distributions were obtained both by deposition on a Pollution Control Systems Mark III cascade impactor, and by filtration and subsequent sizing with a Malvern Instruments particle sizer. Chemical composition of coal minerals and individual ash particles was determined by computer controlled scanning electron microscopy (CCSEM) at the University of Kentucky.

RESULTS AND DISCUSSION

By comparing the initial distribution of minerals present in a pulverized coal with the final distribution of ash particles, it is possible to infer the major mechanisms of mineral transformation occurring. Kentucky #11 was chosen for this study, as it has finely disseminated minerals compared to other bituminous coals, with a relatively low degree of extraneous or excluded mineral matter. As it contains fairly large amounts of illite and kaolinite, it presents an ideal opportunity for examining the transformations undergone by clay minerals in the presence of carbon. The mineralogy of this coal is summarized in Table I.

TABLE I
Kentucky #11 Mineralogy and Ash Composition

Fuel Analysis*		Ash Analysis	
Fixed Carbon	41.9	SiO_2	45.8
Volatile	33.8	Al_2O_3	19.0
Ash	20.3	Fe_2O_3	20.4
Moisture	4.0	CaO	4.4
		MgO	0.9
Mineral Analysis		K_2O	2.5
		Na_2O	0.3
Quartz	19	SO_3	5.2
Kaolinite	8		
Illite	16		
Mix. Silicates	23		
Pyrite	24		

* for as-received coal

Mineral size distributions for this coal were obtained by two techniques: CCSEM analysis of the minerals in the utility grind coal, as well as Malvern analysis of a small sample of the low temperature ash. Results from these two measurements are compared in Fig. 1 with an ash particle size distribution, obtained upon combustion of the coal in 7% oxygen at 1500 K gas temperature. As the curves in the figure indicate, the mineral distributions agreed at small diameters, but varied somewhat at the larger mineral sizes. While the CCSEM indicates 80% by volume of the mineral matter to be < 13 microns in diameter, the low temperature ash measurement indicates that 80% of the mineral matter is less than 30 microns in size. As the two techniques measure size on a different basis (the CCSEM measures a cross-section and infers diameter, while the Malvern is a volume-based technique), this level of agreement is encouraging. Preliminary results with coals having a high percentage of extraneous mineral matter (Kentucky #9 bituminous and San Miguel Texas lignite) yields better agreement across the entire distribution.

Examination of the ash size distribution, measured by a combination of cascade impaction and Malvern techniques and also plotted in Fig. 1, reveals that upon combustion, a large degree of coalescence is taking place. This is evidenced by the uniform shift to larger particle diameters for the entire distribution. Although both char and mineral fragmentation may be occurring, the effects are lost when the utility grind coal is burned and the overall distribution examined. For this coal under these combustion conditions, mineral agglomeration and coalescence dominate.

Examination of the chemical composition of individual ash particles collected under these conditions also suggests that coalescence is the primary mechanism governing ash evolution. Figure 2 presents composition data for all ash particles containing potassium + silicon + aluminum in greater than 80% levels, excluding oxygen. Composition ranges for typical illite and kaolinite particles are also presented. Pure quartz can be assumed to occur at 100% Si on the diagram. Several conclusions can be drawn from this compositional information. First, it is evident that neither pure quartz, illite, nor kaolinite dominate the final ash. The resulting final ash composition is clearly a mixture of these three minerals. The compositions suggest that quartz is incorporated into both clay minerals, though the mixed silicates present in the initial coal are likely contributing as well. Analysis of the data on a particle by particle basis is currently under way to help resolve the effect of the mixed silicates. It is also interesting to note from the Figure that potassium levels do occasionally increase above the baseline present in the initial illite, but it is not a dramatic increase. This observation, coupled with fume measurements reported elsewhere (2), indicates that acid-leachable potassium present in the raw coal can vaporize in addition to being incorporated into the glassy ash particles.

The fate of the pyrite present in the coal can also be deduced from examination of the final ash composition. Mossbauer analyses of ash collected from combustion at two different oxygen levels are presented in Table II. It is evident that only a small portion of the iron is incorporated into a glassy phase under both oxygen levels. As anticipated, the level of iron present as hematite increases as the oxygen level is raised, due to an increase in the kinetically limited magnetite oxidation rate (10).

Table II
Kentucky #11 Mossbauer Results

Conditions	Magnetite	Hematite	Glass
5% O_2, 1500 K	70	21	9
21% O_2, 1500 K	57	33	10

Different behavior was noted in experiments conducted with a North Dakota Beulah lignite coal under this program. This coal was selected both for the large amount of large (>40 micron) pyrite minerals present, and the large amount of acid-leachable calcium. As the size distribution results presented in Fig. 3 indicate, combustion at both 7% and 21% oxygen levels yielded ash particles with distributions shifted toward smaller sizes relative to the initial minerals. What this suggests is that pure minerals may be fragmenting and influencing the distribution. It is anticipated that pyrite is the major species contributing to this observed behavior, as pyrite fragmentation has been noted in the literature under several conditions (11). Further experimentation with both the Beulah lignite and synthetic chars containing only pyrite is under way to test this hypothesis.

SUMMARY

Laboratory combustion experiments conducted with Kentucky #11 bituminous coal at low oxygen levels (7% oxygen in the bulk gas) demonstrate that agglomeration and coalescence of the included minerals is the dominant transformation mechanism occurring. Results suggest a large degree of coalescence is occurring between illite, kaolinite, and quartz minerals, with occasional iron incorporation into the resulting glass. Lack of iron incorporation was demonstrated by Mossbauer measurements, where approximately 10% of the iron was present as a glass under both oxygen levels studied. Acid-leachable potassium occasionally added to the glassy ash, as evidenced by relatively high potassium concentrations in some particles, though vaporization of the acid-leachable potassium was found to occur as well. For the second coal discussed in the study - Beulah lignite - mineral fragmentation was suggested by comparison of the ash distributions with initial mineral distributions measured by CCSEM. This presumably is due to large quantities of large (greater than 40 micron) pyrite present.

ACKNOWLEDGMENTS

The authors thank the Department of Energy Pittsburgh Energy Technology Center for their generous support of this work under contract number DE-AC22-86PC90751. Coal and ash analyses provided by R.W. Bryers of Foster Wheeler, and G.P. Huffman and F.E. Huggins of the University of Kentucky are also gratefully acknowledged.

REFERENCES

1. Bryers, R.W., "An Overview of Slagging/Fouling due to Impurities in Coal," Proceedings of EPRI Conference on Effects of Coal Quality on Power Plants, October (1987).

2. Srinivasachar, S. Helble, J.J., Katz, C.B., and Boni, A.A., "Transformations and Stickiness of Minerals During Pulverized Coal Combustion," Proceedings of the Engineering Foundation Conference on Mineral Matter and Ash Deposition from Coal (in press) (1988).

3. PSI Technology Company, "Transformations of Inorganic Coal Constituents in Combustion Systems," Quarterly Report No. 6, DOE Contract DE-AC22-86PC90751, April (1988).

4. Graham, K.A., Helble, J.J., Kang, S.G., Sarofim, A.F., and Beer, J.M., "Mechanisms of the Transformation of Mineral Matter to Ash in Coal and Model Chars," Proceedings of the Engineering Foundation Conference on Mineral Matter and Ash Deposition from Coal (in press) (1988).

5. Holve, D.J., Comb. Sci. and Tech. 44: 269 (1986).

6. Wibberley, L.J., and Wall, T.F., Comb. Sci. and Tech. 48: 177 (1986).

7. Helble, J.J., and Sarofim, A.F., "Influence of Char Fragmentation on Ash Particle Size Distributions," Comb. and Flame (in press) (1989).

8. Wall, T.F., Bailey, J.G., and Wibberley, L.J., "The Influence of Coal Properties and Combustion Conditions on the Size Distribution of Fly Ash," Proceedings of the Engineering Foundation Conference on Mineral Matter and Ash Deposition from Coal (in press) (1988).

9. Kang, S.G., Helble, J.J., Sarofim, A.F., and Beer, J.M., "Time-Resolved Evolution of Fly Ash During Pulverized Coal Combustion," 22nd Symposium (Int'l) on Combustion, Seattle (in press), August (1988).

10. Srinivasachar, S., and Boni, A.A., "A Kinetic Model for Pyrite Transformations in a Combustion Environment," Fuel (accepted) (1988).

11. Simpson, D.R., and Bond, R.M., "The Behavior of Pyrite and Its Reaction Products During Combustion," Proceedings of the Engineering Foundation Conference on Mineral Matter and Ash Deposition from Coal (in press) (1988).

12. Jorgensen, F.R.A., Trans. Instr. Min. Metall. Sect. C 90: 1 (1981).

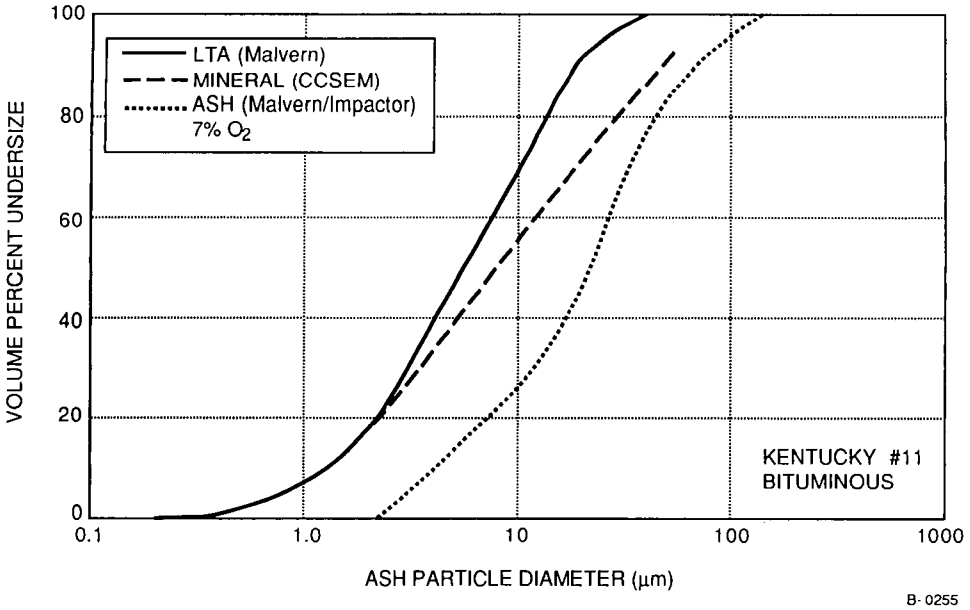

Figure 1: Mineral and Ash Particle Size Distributions - Kentucky #11

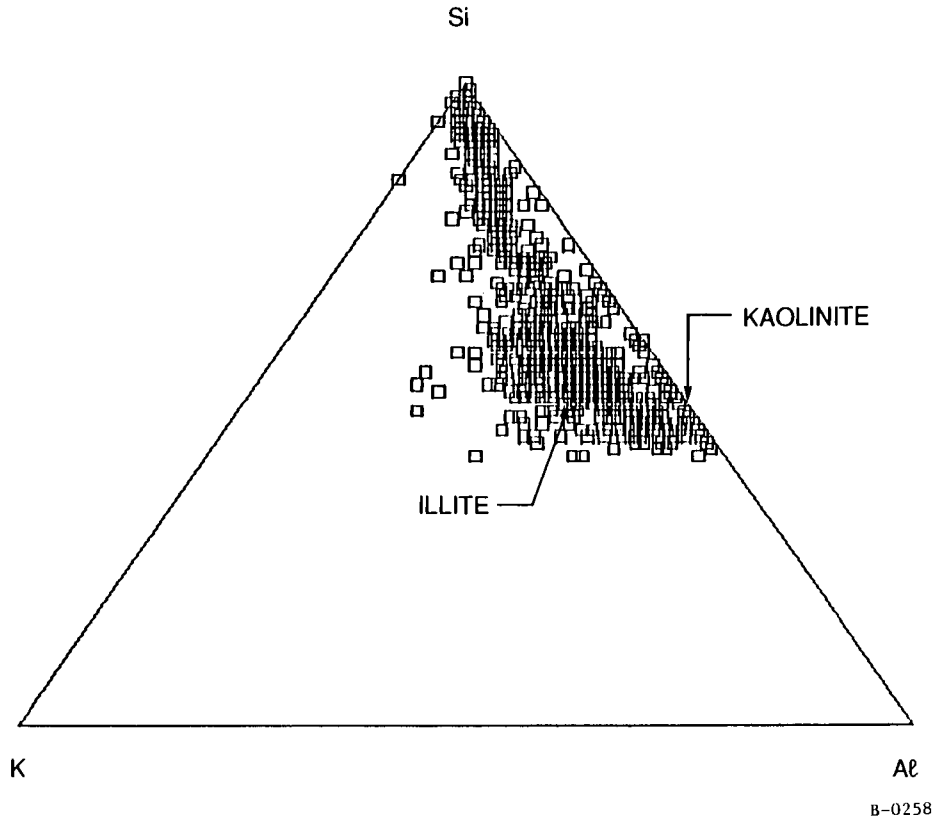

Figure 2: Individual Particle Composition, K+Al+Si>80%, Kentucky #11

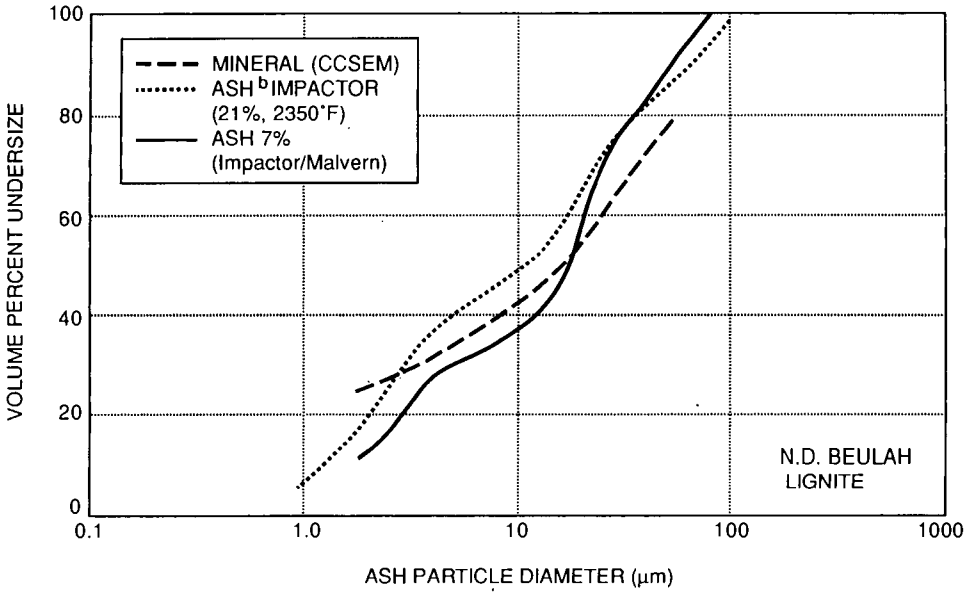

Figure 3: Mineral and Ash Particle Size Distributions - Beulah

A KINETIC DESCRIPTION OF ALKALI TRANSFORMATIONS IN COAL COMBUSTION SYSTEMS

S. Srinivasachar, J.J. Helble, D.O. Ham, and G. Domazetis*
PSI Technology Company
Research Park, P.O. Box 3100
Andover, MA 01810

* State Electricity Commission of Victoria, Australia

ABSTRACT

A kinetic model was developed to predict concentrations of atomic and molecular sodium species existing in both flame and post-flame zones of pulverized coal combustors. To date, the model has successfully predicted measured literature values of sodium species in the $Na/H_2/O_2/N_2$ system. At all but the earliest conditions (< 1 ms) sodium hydroxide is predicted to be the dominant species. Atomic sodium levels decay rapidly, representing less than one percent of the total sodium species present at times greater than 5 milliseconds for lean hydrogen flames (H_2/O_2 = 0.6, temperature = 1650°C). Incorporation of sulfur chemistry into the model did not change this conclusion, as sodium hydroxide was still found to dominate. Further development, however, awaits determination as to whether alkali sulfation occurs in the vapor or the condensed phase, as well as the correct corresponding kinetics. Efforts in these areas are discussed.

BACKGROUND

The release of alkali species during the combustion of pulverized coal can seriously affect both deposition and corrosion of boiler components. Deposition can be affected as follows: Subsequent to combustion, vaporized alkali species will condense on, and possibly interact with, the fly ash particles present in the flue gas. Alkali species are know to reduce the viscosity of silica melts. If this interaction generates ash particles with reduced viscosity below the critical point for deformation and adhesion - a likely result - ash particle deposition may substantially increase, as results have shown that reduced particle viscosities generate increased sticking efficiencies (1,2). Direct condensation of alkali species on cooled tube surfaces may also affect deposition by generating a sticky layer on the tube surface, thereby increasing the sticking efficiency of impacting ash particles. Corrosion can also be directly affected by condensation of alkali species on the boiler tube surfaces. Clearly, the extent of influence the alkali species exert on the deposition and corrosion processes will depend upon the particular species present, as the various alkali compounds have different vapor pressures and hence will condense at different temperatures (locations) within a boiler.

Although it is accepted that the atomic alkali species is the vaporizing species during combustion (except for coals with high sodium chloride

content, in which case it is also as the chloride), it is presently unclear when transformations to molecular oxide species occur, and at what point the assumption of equilibrium is valid. For this reason, a kinetics scheme was developed to follow the transformations of atomic sodium in a combustion environment. The model, which employs the CHEMKIN chemical kinetics code to solve the complex series of reactions, has been used to reproduce species profiles for $H_2/O_2/N_2/Na$ flames appearing in the literature. Modified species profiles resulting from addition of sulfur to the reaction chemistry, utilizing the preliminary sulfation kinetics scheme proposed by Domazetis and Campisi (3), have also been generated, and are discussed herein.

SODIUM VAPORIZATION

Sodium may occur in several forms within a given coal. It may be present as NaCl inclusions, less frequently as small Na_2SO_4 inclusions, or as organically bound material directly attached to the coal structure via carboxylic acid groups. Both of these forms readily vaporize under the high temperature environment of coal combustion, generating atomic sodium and/or NaCl in the vapor phase. Sodium also frequently appears as a component in the clay minerals such as plagioclase, $NaCaAlSiO_x$, contained in coals, though thermodynamic calculations have indicated that sodium has low activity in sodium - silica melts (4), thus suggesting that it may be relatively inert to vaporization in this form.

Vaporization of both the chloride and organic forms of sodium occurs rapidly at temperatures well below peak flame temperature, as measured by atomic absorption at SECV and shown in Fig. 1. Sodium carboxylates dissociate in the range 400 to 800°C, forming Na_2CO_3, which subsequently decomposes further to form atomic Na at temperatures below 900°C. Sodium chloride also vaporizes rapidly under these conditions. Calculations indicate that in the temperature range 1000 - 1100°C, NaCl will completely vaporize in approximately 10 ms, and hence before char oxidation is fully under way. Vaporization of NaCl resulting from reduction to the volatile metallic form may compete with this process, via the reaction (3)

$$NaCl + coal\ /\ volatiles \rightarrow Na\ (g) + HCl\ (g) \qquad (1)$$

Upon vaporization, the atomic Na quickly encounters the complex chemical environment surrounding the reacting particle. Many species, including H, OH, CO, O, and H_2O are present in this environment, and may potentially affect the conversion of sodium to bound molecular states. Work in laboratory hydrogen flat flames has indicated this to be true, as experimental measurements of Na and OH coupled with kinetic modeling in lean flames demonstrated that Na profiles roughly track the decay of H atoms (5). In that study, the authors demonstrated that despite the existence of some twenty forward/reverse reactions affecting sodium species in their hydrogen flame, the complex sodium chemistry was dominated by just four reactions:

$$Na + H_2O = NaOH + H \quad (2)$$

$$Na + O_2 + M = NaO_2 + M \quad (3)$$

$$NaO_2 + H = NaO + OH \quad (4)$$

$$NaOH + OH = NaO + H_2O \quad (5).$$

MODEL DEVELOPMENT AND RESULTS

By utilizing these four reactions in conjunction with a detailed hydrogen oxidation reaction sequence (6), CHEMKIN was used to determine species concentration levels for comparison to the data of reference (5). Note that the authors of reference (5) successfully modeled the kinetics in their study using measured OH as an input; in the model described and tested herein, OH is a predicted quantity. For typical lean flame data of $H_2/O_2/N_2$ equal to 0.6/1/1, corresponding to an average measured temperature of 1917 K (6), sodium levels are predicted to decay rapidly. As the curves in Figure 2 demonstrate, this decay parallels the rapid decrease in atomic hydrogen concentration. Sodium hydroxide is seen to be the dominant sodium compound at all times greater than 0.5 ms, as predicted by the measurements and calculations in reference 5.

Calculations were repeated under higher temperature conditions, where $H_2/O_2/N_2$ ratios of 1.8/1/3 yielded flame temperature of 2350 K. Under these conditions (results not shown), atomic sodium persisted for longer periods of time, and was present in levels comparable to NaOH. Again, the concentration profiles predicted here agree closely with those measured (OH and Na) and predicted by the investigators of the aforementioned study.

Calculations were also carried out subsequent to the incorporation of sulfur into the reaction matrix. Sodium-sulfur species are of prime interest in this study, as they are thought to play a major role in initiating deposition in the cooler regions of utility boilers. Although several studies have indicated the major sodium - sulfur reaction to be (7)

$$NaOH + SO_2 = NaSO_2 + OH \quad (6)$$

the entire sulfur reaction sequence, including all anticipated reactions with H, OH, and O was incorporated into the kinetic model discussed herein. Values for the reaction rate coefficients for this set of reactions were obtained from Domazetis and Campisi (3).

The effect of low levels of sulfur (0.4% by volume) on the sodium reaction chemistry can be seen by comparing species concentrations in Figure 2 with those presented in Figure 3, which includes sulfur. Temperature was assumed equal in both calculations, as the small amount of sulfur added will have a negligible effect. At 1917 K for the $H_2/O_2/N_2$ levels considered previously,

NaOH is still seen to be the dominant sodium species. Both $NaSO_2$ and NaO_2 are also predicted to occur, but at only 1% of the level of NaOH.

Although vapor phase Na_2SO_4 was considered in the reaction sequence, the calculations performed to date suggest that it will not form under these flame conditions. The possibility has not been excluded, however, as we have not yet identified a fundamental kinetic mechanism which permits the formation of Na_2SO_4 based upon collisions of gas phase species. This raises an interesting point as to the exact origin of sodium sulfate, as sodium sulfate is often identified in boiler deposits, and is frequently assumed to be the cause of initiation of convective pass fouling. The limited experimental data available to date indicate that vapor phase sodium sulfate may indeed form at flame conditions (not specified) (8), as determined by molecular beam mass spectrometry, though further evidence including a plausible kinetics scheme has not been presented. An independent set of calculations (3) suggest another mechanism for formation of Na_2SO_4 in the "vapor," as a result of complexing of species such as NaOH and $NaSO_2$ during condensation. This proposed non-elementary formation process has not been verified experimentally.

Efforts are currently under way on several fronts in the coal combustion community in an effort to conclusively determine the point (and phase) of alkali sulfation. Atomic sodium release and oxidation in coal systems is being studied through atomic laser-induced fluorescence (9), while at PSIT, techniques which permit direct measurement of alkali chloride and hydroxide in the vapor phase (10) are being employed in a combustion experiment to determine the location of sulfation. Traditional combustion experiments geared toward inducing preferential condensation of the sulfate are also under way at PSIT.

SUMMARY

In summary, a kinetic model utilizing sodium reaction sequences and rate coefficients from the literature has been incorporated into CHEMKIN. The model was able to successfully predict literature values of species concentrations in lean $H_2/O_2/N_2$ flames doped with sodium. Extension of the model to incorporate gas phase sulfur chemistry suggested that NaOH will still dominate under oxygen rich atmospheres, though NaO_2 and $NaSO_2$ will also form. The absence of vapor phase Na_2SO_4 suggests that Na_2SO_4 formation is a condensed phase reaction, though further mechanistic information is required before this can be conclusively determined. The possible existence of this species under other conditions is currently under investigation experimentally, as conclusive determination of the phase in which reaction to form alkali sulfate occurs remains to be accomplished.

ACKNOWLEDGMENTS

The authors gratefully acknowledge the financial support of the Department of Energy, Pittsburgh Energy Technology Center, through contract number DE-AC22-86PC90751. The authors also wish to thank the State Electricity

Commission of Victoria for generously providing funds which permitted Dr. Domazetis to interact with PSIT researchers during the course of this work.

REFERENCES

1. Srinivasachar, S., Helble, J.J., Katz, C.B., and Boni, A.A., "Transformations and Stickiness of Minerals During Pulverized Coal Combustion," Proceedings of the Engineering Foundation Conference on Mineral Matter and Ash Deposition from Coal (in press) (1988).

2. PSI Technology Company, "Transformations of Inorganic Coal Constituents in Combustion Systems," Quarterly Report Number 6, DOE Contract DE-AC22-86PC90751, April (1988).

3. Domazetis, G., and Campisi, A., "Chemical Kinetics of Coal Combustion and Pollution Formation," State Electricity Commission of Victoria, Report Number SO/86/104, Project No. 2403, NERDDP 933 (1986).

4. PSI Technology Company, "Transformations of Inorganic Coal Constituents in Combustion Systems," Quarterly Report Number 4, DOE Contract DE-AC22-86PC90751, October (1987).

5. Hynes, A.J., Steinberg, M., and Schofield, K., "The Chemical Kinetics and Thermodynamics of Sodium Species in Oxygen-Rich Hydrogen Flames," J. Chem. Phys. 80: 2585 (1984).

6. Muller, C.H., Schofield, K., Steinberg, M., and Broida, H.P., "Sulfur Chemistry in Flames," Seventeenth Symposium (Int'l) on Combustion, The Combustion Institute, Pittsburgh, p. 867 (1979).

7. Fenimore, C.P., "Two Modes of Interaction of NaOH and SO_2 in Gases From Fuel-Lean H_2-Air Flames," Fourteenth Symposium (Int'l) on Combustion, The Combustion Institute, Pittsburgh, p. 955 (1973).

8. Greene, F.T., and O'Donnel, J.E., "Investigation of Mechanisms of Ash Deposit Formation From Low-Rank Coal Combustion," Final Report of DOE Contract No. DE-AC21-81FC10287 by Midwest Research Institute, August (1987).

9. University of North Dakota Energy and Minerals Research Center, "Combustion Inorganic Transformations," Quarterly Report No. 8 under DOE Cooperative Agreement DE-FC21-86MC-10637, April (1988).

10. Oldenborg, R., "Optical Detection of Corrosive Compounds," paper presented at DOE AR&TD Direct Utilization and Instrumentation & Diagnostics Contractors' Review Meeting, Pittsburgh, September (1988).

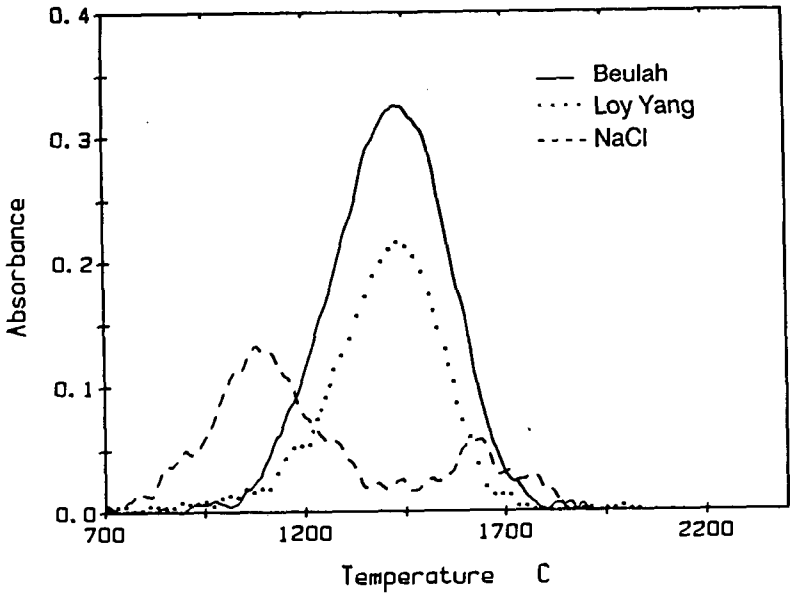

Figure 1 - Atomic Na formation profiles from Beulah and Loy Yang coals by AA

H_2 / O_2 / N_2 / S
0.6 / 1.0 / 1.0 / 0.01

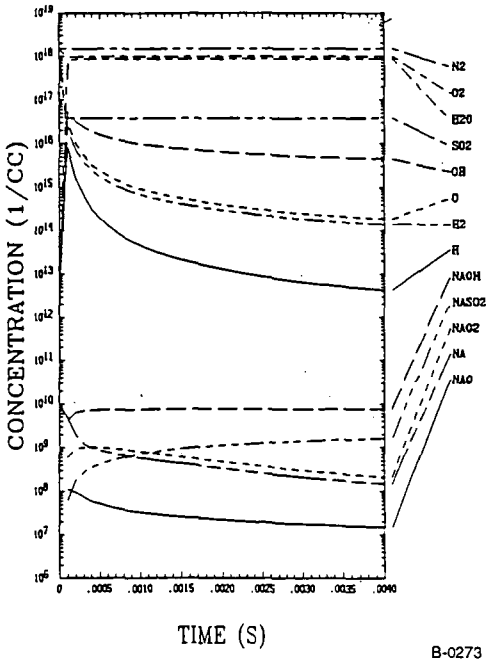

Figure 2 Model Predictions Without Sulfur

H_2 / O_2 / N_2 / S
0.6 / 1.0 / 1.0 / 0.00

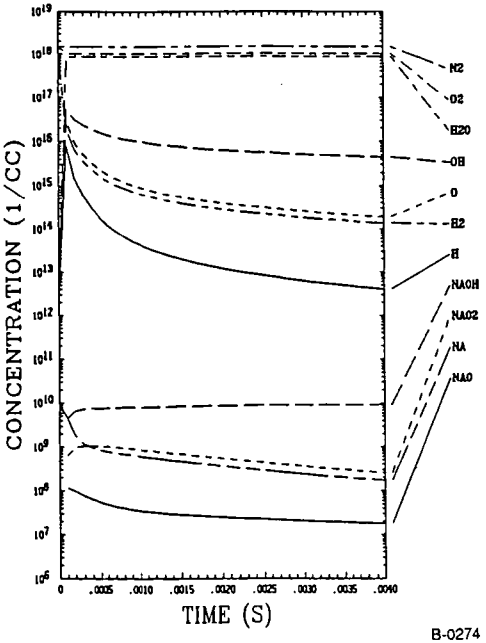

Figure 3: Model Predictions Incorporating Sulfur